Fast Microwave Medical Imaging Based on Iterative Smoothed Adaptive Thresholding

Masoumeh Azghani, Panagiotis Kosmas, and Farokh Marvasti

***Abstract*—This letter presents a fast microwave imaging technique based on the concept of smoothed minimization and adaptive thresholding. The distorted Born iterative method (DBIM) is used to solve the electromagnetic (EM) inverse scattering problem. We propose to solve the set of underdetermined equations at each iteration of the DBIM algorithm using an L_2 regularized iterative smoothed adaptive thresholding (L_2-ISATCS) technique. Our simulation results confirm that this technique can reduce considerably the required reconstruction times for the DBIM method relative to previously suggested compressed sensing (CS)-based approaches.**

***Index Terms*—Adaptive thresholding, breast imaging, compressed sensing, inverse scattering, microwave tomography.**

I. Introduction

THE MAIN goal of microwave tomography is to estimate the location of scatterers (e.g. tumors) in biological tissue by recovering the distribution of the dielectric properties. This is achieved by solving an electromagnetic (EM) inverse scattering problem [1]. Various optimization techniques such as the conjugate gradient (CG) [2], [3] and Gauss–Newton (GN) [4]–[6] methods have been applied to solve the EM inverse scattering problem.

GN algorithms can be implemented via the distorted Born iterative method (DBIM), which solves the nonlinear EM inverse scattering problem by approximating it with successive underdetermined sets of linear equations [3], [7]. The linear problem at each DBIM iteration can be solved by various methods including techniques [7], [8] inspired by compressed sensing (CS) theory [9], [10]. In recent work, we have proposed the application of the L_2-IMATCS algorithm, which applies the majorization minimization technique to solve the L_2-regularized L_0 minimization problem with the use of adaptive thresholding [7].

In this letter, an L_2-regularized iterative smoothed adaptive thresholding based on compressed sensing (L_2-ISATCS) technique is proposed for the solution of the L_2-regularized L_0 minimization problem in microwave imaging (MWI). The goal of the proposed scheme is to minimize a smoothed version of the cost function that is differentiable. The minimization technique consists of two major steps, a gradient descent update equation, and a projection onto a sparse domain based on adaptive thresholding. The smoothing of the cost function has a good effect on the stability of the problem. More importantly, the convergence of the algorithm is greatly accelerated by combining adaptive thresholding and smoothed minimization. This is confirmed by the presented simulation cases that demonstrate the much faster convergence and comparable accuracy of the proposed technique to the L_2-IMATCS algorithm proposed in our previous work [7].

The remainder of the letter is structured as follows. Section II presents the mathematical formulation for our new CS-based algorithm based on smoothed adaptive thresholding. Section III presents results from a set of simulations that we have used previously to evaluate our CS techniques [7]. These results demonstrate the considerably faster convergence of the proposed method. Finally, a short conclusion is given in Section IV.

II. L_2-ISATCS Technique

A detailed formulation of the CS-based EM inverse scattering problem is given in our previous work [7]. Here, we describe the proposed L_2-ISATCS technique to solve the linear problem at each DBIM iteration. The cost function to be minimized in this problem is

$$\|\mathbf{y}-\mathbf{A}\mathbf{x}\|_2^2+\lambda_1\|\mathbf{x}\|_0+\lambda_2\|\mathbf{x}\|_2^2 \tag{1}$$

where the first term represents the error. The minimization of the L_0 norm encourages sparsity, and the L_2 norm stabilizes the algorithm. The above cost function is nonsmooth and nondifferentiable. Hence, the implementation of minimization techniques is not straightforward. To address this problem, we suggest to use a smoothed approximation of the cost function. The smoothed cost function to be minimized is then given as

$$\Phi(\mathbf{x})=\|\mathbf{y}-\mathbf{A}\mathbf{x}\|_2^2+\lambda_1\sum_{i=1}^{n}H(\mathbf{x}_i)+\lambda_2\|\mathbf{x}\|_2^2. \tag{2}$$

The function $\sum_{i=1}^{n}H(\mathbf{x}_i)$ is a smoothed approximation of the L_0 norm. We note that the concept of smoothed L_0 minimization has previously been applied in compressed sensing recovery in [11] and [12]. Among various candidates, we use an exponential smoothing function given by

$$H(\mathbf{x}_i)=\exp-\frac{\mathbf{x}_i^2}{2\sigma^2} \tag{3}$$

Manuscript received October 15, 2014; accepted October 25, 2014. Date of publication November 03, 2014; date of current version February 05, 2015.

M. Azghani and F. Marvasti are with the Advanced Communications Research Institute (ACRI), Electrical Engineering Department, Sharif University of Technology, Tehran, Iran (e-mail: azghani@ee.sharif.ir; marvasti@sharif.edu).

P. Kosmas is with the School of Natural and Mathematical Sciences, King's College London, London WC2R 2LS, U.K. (e-mail: panagiotis.kosmas@kcl.ac.uk).

Color versions of one or more of the figures in this letter are available online at http://ieeexplore.ieee.org.

Digital Object Identifier 10.1109/LAWP.2014.2366919

where σ controls the precision of the approximation, i.e., a smaller σ increases accuracy in the approximation. However, reducing the value of σ also reduces the smoothness of the cost function, thereby increasing the number of its local minima and making the algorithm susceptible to errors. To handle this issue, we decrease the value of the parameter σ gradually at each iteration. The following two-step technique minimizes the smoothed cost function:

- The first step: Decrease the cost function by moving toward the minus of its gradient.
- The second step: Adaptively threshold the gradient descent result to project the solution to the space of sparse vectors.

The adaptive thresholding operator accelerates the convergence of the algorithm, as confirmed through our simulation results in Section III.

The gradient function is obtained as

$$\nabla\Phi\left(\mathbf{x}^k\right) = \mathbf{A}^T\left(\mathbf{A}\mathbf{x}^k - \mathbf{y}\right) + \lambda_1 h\left(\mathbf{x}^k\right) + 2\lambda_2\mathbf{x}^k \quad (4)$$

where the vector function h indicates the gradient of the smoothed L_0 function

$$h\left(\mathbf{x}_i\right) = \frac{\mathbf{x}_i}{\sigma^2}\exp -\frac{\mathbf{x}_i^2}{2\sigma^2} \quad (5)$$

Thus, the aforementioned two-step algorithm can be summarized as,

$$\mathbf{x}^{k+1} = T^k\left(\mathbf{x}^k - \mu\nabla\Phi\left(\mathbf{x}^k\right)\right) \quad (6)$$

where $T^k(.)$ is the adaptive thresholding operator as

$$T^k(z) = \begin{cases} z, & |z| \geq \theta(k) \\ 0, & |z| < \theta(k). \end{cases} \quad (7)$$

The threshold value $\theta(k)$ is changed adaptively with the iteration number as

$$\theta(k) = \theta(0)e^{-\alpha k}. \quad (8)$$

Finally, the resultant iterative relation follows

$$\mathbf{x}^{k+1} = T^k\left(\left(1-2\lambda_2\right)\mathbf{x}^k + \mu\left(\mathbf{A}^T\left(\mathbf{y}-\mathbf{A}\mathbf{x}^k\right) - \lambda_1 h\left(\mathbf{x}^k\right)\right)\right). \quad (9)$$

The details of the iterative smoothed adaptive thresholding technique are illustrated in Algorithm 1. The outer loop in this algorithm gradually decreases the value of σ, and the inner loop implements the iterative relation of the L_2-ISATCS scheme.

Algorithm 1: L_2-regularized Iterative Smoothed Adaptive Thresholding based on Compressed Sensing (L_2-ISATCS)

input:
A measurement matrix $\mathbf{A} \in \mathbb{R}^{m\times n}$
A measurement vector $\mathbf{y} \in \mathbb{R}^m$
The maximum number of iterations K
output:
A recovered estimate $\widehat{\mathbf{x}} \in \mathbb{R}^n$ of the original signal.
procedure L_2-ISATCS(y, x)
  $\mathbf{x}^0 \leftarrow 0$
  $\sigma \leftarrow \sigma_0$
  for $k = 1 : K$ **do**
    $\sigma \leftarrow 0.8\sigma$
    $\mathbf{x}^{k+1} \leftarrow T^k((1-2\lambda_2)\mathbf{x}^k + \mu(\mathbf{A}^T(\mathbf{y}-\mathbf{A}\mathbf{x}^k) - \lambda_1 h(\mathbf{x}^k)))$
  end for
  return $\widehat{\mathbf{x}} \leftarrow \mathbf{x}^K$
end procedure

III. Simulation Results

As in our previous work [7], we use the finite-difference time-domain (FDTD) method with a uniform grid cell size of 2.0 mm to simulate measured data, and also as forward solver for the DBIM algorithm. We also use the same numerical breast models and dispersive breast tissue properties as in [7], taken from from the University of Wisconsin (UW)-Madison's repository [13]. We note that this 2.0-mm cell size is dictated by the resolution of the (coarse) breast model; the actual resolution of our imaging method depends on the employed frequency range and the regularization method used within the DBIM [6]. Our imaging algorithms estimate the parameters ϵ_∞, ϵ_s, and σ_s of the Debye model for the complex relative permittivity

$$\epsilon_\mathrm{r}(\omega) = \epsilon_\infty + \frac{\epsilon_\mathrm{s} - \epsilon_\infty}{1 + j\omega\tau} - j\frac{\sigma_\mathrm{s}}{\omega\epsilon_0}. \quad (10)$$

In all of the simulations, the parameter τ is set to 17.1 and a lossless background medium is considered with $\epsilon_\mathrm{r} = 2.6$. The data has been captured from six equally spaced frequencies in the range 1.2–2.7 GHz.

We have shown the advantages of the L_2-IMATCS over competing approaches such as the elastic net [8] in our previous paper [7]. Hence, in this work, we consider the L_2-IMATCS as a benchmark of the proposed L_2-ISATCS algorithm. For a fair comparison, we have used the same thresholding parameters for the L_2-IMATCS and L_2-ISATCS schemes that are: $\theta(0) = 0.07$, $\alpha = 0.04$, and $K = 100$ (which result in further improvement in the L_2-IMATCS reconstructions relative to [7]). The parameters μ and λ_1 are set to 0.001 and 1.9 for the L_2-ISATCS implementation. The choice and impact of these parameters as well as the effect of the properties of the background medium and the initial guess for the imaging algorithm have been analyzed in our previous work [7].

We first consider the testbeds shown in Fig. 1 [7], which feature closely spaced targets that cannot be resolved with traditional L_2 regularization schemes [6]. In the simulation results reported here, we have considered 16 antennas surrounding the breast as shown in Fig. 1(a).

Reconstructions from the L_2-ISATCS and L_2-IMATCS algorithms are presented in Fig. 2, which shows that the L_2-ISATCS technique resolves the two targets with somewhat higher accuracy. We have also repeated this simulation scenario including Gaussian noise added to the measurements. Results for signal-to-noise ratios (SNRs) of 30 and 60 dB are shown in Fig. 3. As in our previous work [7], the conductivity values are estimated

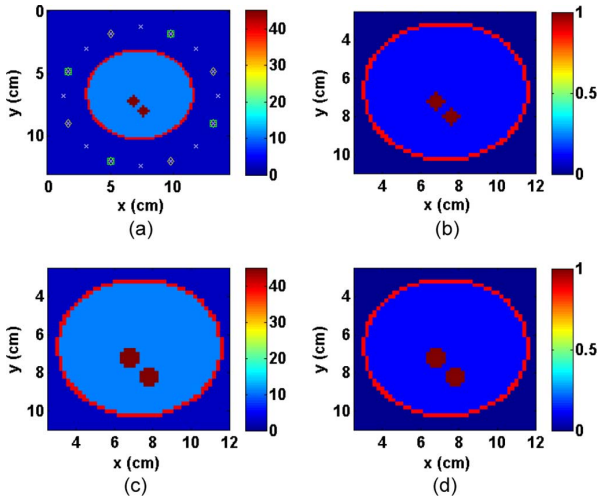

Fig. 1. Maps of (a), (c) the dielectric constant ϵ_r and (b), (d) the conductivity σ calculated at 1 GHz for the two simulation scenarios with targets of different size and shape.

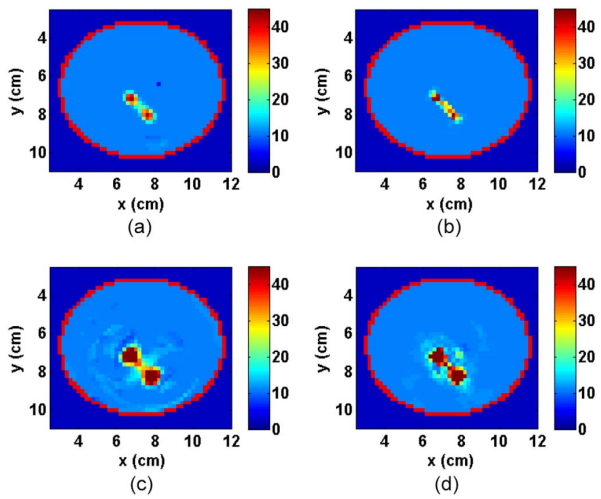

Fig. 2. Reconstructed dielectric constant ϵ_r distribution calculated at 1 GHz for (a), (c) the L_2-ISATCS and (b), (d) the L_2-IMATCS algorithms and the two cases of Fig. 1 using the 16 antennas depicted in Fig. 1(a).

with somewhat lower accuracy than the permittivity shown in these figures, but the two images are highly correlated since we are effectively reconstructing the Debye parameters in (10). A slightly greater deterioration in the estimated conductivity values for the L_2-ISATCS relative to L_2-IMATCS occurs in the case of SNR $=$ 30 dB. This is quantified in Table I, which calculates the normalized error norm of the difference between the reconstructed and the true permittivity and conductivity distributions for the cases of Figs. 2 and 3.

The convergence performance of the suggested technique is illustrated by depicting the data residual norm $\|\mathbf{y}-\mathbf{A}\mathbf{x}\|$ versus DBIM iteration number in Fig. 4. The residual error curve of the L_2-ISATCS is always below that of the L_2-IMATCS algorithm until they eventually converge to almost equal values. Importantly, the plot shows that the convergence rate of the proposed L_2-ISATCS scheme is considerably higher than that of L_2-IMATCS, requiring about 50% less iterations. Similar results are obtained for other scenarios such as the case of eight

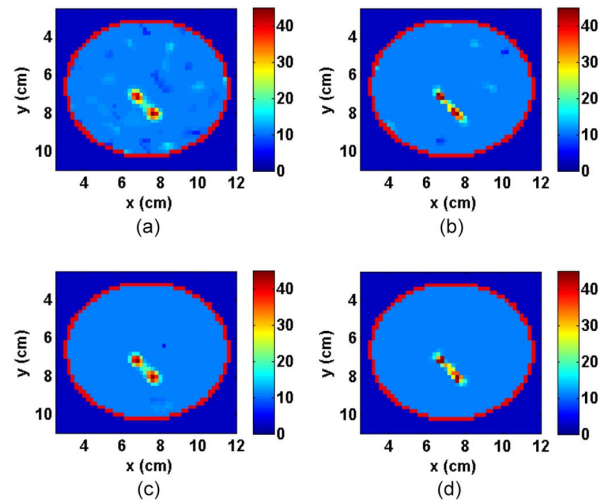

Fig. 3. Reconstructed dielectric constant ϵ_r distribution calculated at 1 GHz for the top case in Fig. 1: (a) L_2-ISATCS with SNR $=$ 30 dB; (b) L_2-IMATCS with SNR $=$ 30 dB; (c) L_2-ISATCS with SNR $=$ 60 dB; (d) L_2-IMATCS with SNR $=$ 60 dB.

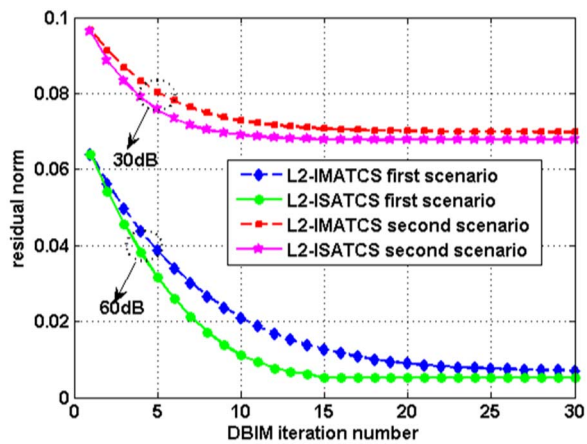

Fig. 4. Norm of the residual data vector $\|\mathbf{y}-\mathbf{A}\mathbf{x}\|$ versus DBIM iteration number for the reconstructions of Fig. 3, where first and second scenarios correspond to SNR of 60 and 30 dB, respectively.

TABLE I
MEAN SQUARE ERROR (MSE) NORMS ("TRUE"-"RECONSTRUCTED") AT 1 GHZ

scenario	parameter	L2-ISATCS	L2-IMATCS
Fig. 2-top	ϵ_r	0.1718	0.1998
	σ	0.0039	0.0040
Fig. 2-bottom	ϵ_r	0.2461	0.2383
	σ	0.0131	0.0103
Fig. 3-top (SNR=30 dB)	ϵ_r	0.2238	0.2036
	σ	0.0083	0.0038
Fig. 3-bottom (SNR=60 dB)	ϵ_r	0.1720	0.1973
	σ	0.0038	0.0040

antennas surrounding the breast [the squares in Fig. 1(a)], thus confirming the improved convergence of the L_2-ISATCS over the L_2-IMATCS algorithm.

As in [7], we have also examined the algorithm's performance for more realistic imaging scenarios based on a 2-D coronal slice of a heterogeneous breast phantom obtained from UW-Madison's dataset [13] (see Fig. 5). The performance of the proposed scheme and the L_2-IMATCS technique has again

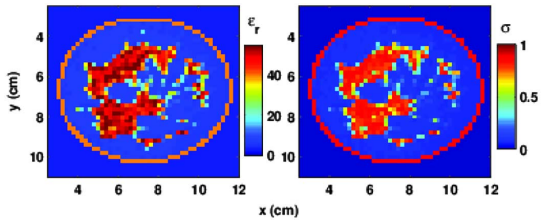

Fig. 5. Maps of *(left)* the dielectric constant ϵ_r and *(right)* the conductivity σ calculated at 1 GHz for the full-breast simulation testbed. The spatial resolution is 2 mm.

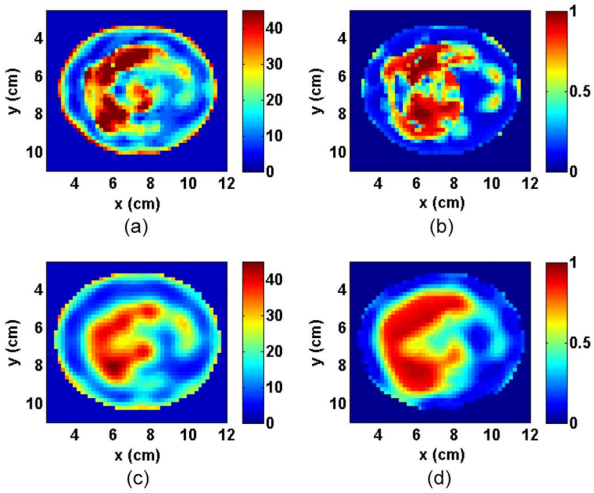

Fig. 6. Reconstructed permittivity and conductivity distributions calculated at 1 GHz for the full breast model of Fig. 5 and eight antennas. (a) ϵ_r for the L_2-ISATCS; (b) σ for the L_2-ISATCS; (c) ϵ_r for the L_2-IMATCS; (d) σ for the L_2-IMATCS.

been compared for noise-free and noisy data with SNRs of 30 and 60 dB relative to the total received signal. Examples of the permittivity and conductivity images resulting from the two algorithms are shown in Fig. 6 for noise-free data and eight antennas. In addition to producing higher-resolution images, the L_2-ISATCS method converges in as few as eight DBIM iterations, while the L_2-IMATCS requires 30 iterations to converge. This considerably faster convergence of the L_2-ISATCS scheme has been observed for all cases and is very important for reducing the overall computational cost of the DBIM, which increases linearly with the iteration number.

In addition to improving the overall DBIM convergence significantly, the proposed algorithm also leads to a faster solution of the linear problem at each DBIM iteration. To demonstrate this, we have computed the average CPU time required per DBIM iteration for the two algorithms implemented using MATLAB. Results for the presented simulations are given in Table II, where computations have been performed on a standard PC environment (Intel Core i7-4930 K CPU at 3.4 GHz, RAM 16 GB). As shown in the table, the CPU time for running the L_2-ISATCS algorithm is on average about 23 times less than the CPU time required for the L_2-IMATCS.

IV. Conclusion

This letter introduced a fast microwave medical imaging technique based on smoothed adaptive thresholding. In order to promote sparsity, a smoothed approximation of the L_0 semi-norm was considered. Moreover, the L_2 regularizer was adopted to cope with the instabilities occurred in the EM inverse scattering problem. The resultant cost function was minimized using a gradient descent step followed by an adaptive thresholding operator that speeds up the algorithm. Various simulation scenarios have been explored in this work, which confirm that the proposed L_2-ISATCS technique can improve considerably the convergence rate of the DBIM. In addition, the L_2-ISATCS implementation is less computationally costly than our previous L_2-IMATCS implementation. These benefits are very important for computationally intensive three-dimensional (3-D) reconstructions, which will be the topic of our future work.

TABLE II
Average Simulation Time per DBIM Iteration in Seconds

Scenario	L2-IMATCS	L2-ISATCS
The bottom case of Fig. 1	2.74	0.11
The top case of Fig. 1	2.80	0.12
The top case of Fig. 1 with SNR of 30 dB	2.60	0.11
The top case of Fig. 1 with SNR of 60 dB	2.65	0.13
The heterogeneous model with SNR of 30 dB	2.71	0.12
The heterogeneous model with SNR of 60 dB	2.63	0.11

References

[1] S. Semenov, "Microwave tomography: Review of the progress towards clinical applications," *Philos. Trans. Royal Soc. A*, vol. 367, pp. 3021–3042, 2009.
[2] C. Gilmore, A. Abubakar, W. Hu, T. M. Habashy, and P. M. van den Berg, "Microwave biomedical data inversion using the finite-difference contrast source inversion method," *IEEE Trans. Antennas Propag.*, vol. 57, no. 5, pp. 1528–1538, May 2009.
[3] R. Scapaticci, I. Catapano, and L. Crocco, "Wavelet-based adaptive multiresolution inversion for quantitative microwave imaging of breast tissues," *IEEE Trans. Antennas Propag.*, vol. 60, no. 8, pp. 3717–3726, Aug. 2012.
[4] P. M. Meaney *et al.*, "Initial clinical experience with microwave breast imaging in women with normal mammography," *Acad. Radiol.*, vol. 14, no. 2, pp. 207–218, Feb. 2007.
[5] J. D. Shea, P. Kosmas, S. C. Hagness, and B. D. Van Veen, "Three-dimensional microwave imaging of realistic numerical breast phantoms via a multiple-frequency inverse scattering technique," *Med. Phys.*, vol. 37, no. 8, p. 4210, Aug. 2010.
[6] P. Kosmas, J. D. Shea, B. D. Van Veen, and S. C. Hagness, "Three-dimensional microwave imaging of realistic breast phantoms via an inexact Gauss-Newton algorithm," in *Proc. IEEE APS-URSI*, Jul. 2008, pp. 1–4.
[7] M. Azghani, P. Kosmas, and F. Marvasti, "Microwave medical imaging based on sparsity and an iterative method with adaptive thresholding," *IEEE Trans. Med. Imag.*, 2014, to be published.
[8] D. W. Winters, B. D. Van Veen, and S. C. Hagness, "A sparsity regularization approach to the electromagnetic inverse scattering problem," *IEEE Trans. Antennas Propag.*, vol. 58, no. 1, pp. 145–154, Jan. 2010.
[9] E. J. Candes and M. B. Wakin, "An introduction to compressive sampling," *IEEE Signal Process. Mag.*, vol. 25, no. 2, pp. 21–30, Mar. 2008.
[10] D. L. Donoho, "Compressed sensing," *IEEE Trans. Inf. Theory*, vol. 52, no. 4, pp. 1289–1306, Apr. 2006.
[11] H. Mohimani, M. Babaie-Zadeh, and C. Jutten, "A fast approach for overcomplete sparse decomposition based on smoothed norm," *IEEE Trans. Signal Process.*, vol. 57, no. 1, pp. 289–301, Jan. 2009.
[12] J. Trzasko and A. Manduca, "Highly undersampled magnetic resonance image reconstruction via homotopic-minimization," *IEEE Trans. Med. Imag.*, vol. 28, no. 1, pp. 106–121, Jan. 2009.
[13] E. Zastrow *et al.*, "Development of anatomically realistic numerical breast phantoms with accurate dielectric properties for modeling microwave interactions with the human breast," *IEEE Trans. Biomed. Eng.*, vol. 55, no. 12, pp. 2792–2800, Dec. 2008.